Terr. Atmos. Ocean. Sci., Vol. 21, No. 3, 409-428, June 2010 doi: 10.3319/TAO.2009.11.13.01(TH)

Growth Normal Faulting at the Western Edge of the Metropolitan Taipei Basin since the Last Glacial Maximum, Northern Taiwan

Chih-Tung Chen[1], Jian-Cheng Lee[2, *], Yu-Chang Chan[2], and Chia-Yu Lu[1]

[1] *Department of Geosciences, National Taiwan University, Taipei 106, Taiwan, ROC*
[2] *Institute of Earth Sciences, Academia Sinica, Taipei 115, Taiwan, ROC*

Received 25 April 2008, accepted 13 November 2009

ABSTRACT

Growth strata analysis is an useful tool in understanding kinematics and the evolution of active faults as well as the close relationship between sedimentation and tectonics. Here we present the Shanchiao Fault as a case study which is an active normal fault responsible for the formation of the 700-m-thick late Quaternary deposits in Taipei Basin at the northern tip of the Taiwan mountain belt. We compiled a sedimentary record, particularly the depositional facies and their dated ages, at three boreholes (SCF-1, SCF-2 and WK-1, from west to east) along the Wuku Profile that traverses the Shanchiao Fault at its central segment. By incorporating the global sea level change curve, we find that thickness changes of sediments and changes of depositional environments in the Wuku area are in a good agreement with a rapid sea level rise since the Last Glacial Maximum (LGM) of about 23 ka. Combining depositional facies changes and their ages with their thickness, we are able to introduce a simple back-stripping method to reconstruct the evolution of growing strata across the Shanchiao Fault since the LGM. We then estimate the vertical tectonic slip rate since 23 ka, which exhibits 2.2 mm yr^{-1} between SCF-2 and WK-1 and 1.1 mm yr^{-1} between SCF-1 and SCF-2. We also obtain the Holocene tectonic subsidence rate of 2.3 mm yr^{-1} at WK-1 and 0.9 mm yr^{-1} at SCF-2 since 8.4 ka. We thus conclude that the fault zone consists of a high-angle main fault to the east between SCF-2 and WK-1 and a western lower-angle branch fault between SCF-1 and SCF-2, resembling a tulip structure developed under sinistral transtensional tectonism. We find that a short period of 600-yr time span in 9 - 8.4 ka shows important tectonic subsidence of 7.4 and 3.3 m for the main and branch fault, respectively, consistent with possible earthquake events proposed by previous studies during that time. A correlation between geomorphology and subsurface geology in the Shanchiao Fault zone shows that an array of subtle geomorphic scarps corresponds to the branch fault, however, that the surface trace of the main fault seems to be completely erased by the surface force of erosion and sedimentation. We recommend that analysis in the light of growth-faulting scheme should be conducted in a more systematic way for earthquake geology study in other portions of the Shanchiao Fault within the Taipei Basin, as well as other areas worldwide currently under extensional deformation.

Key words: Growth faulting, the Shanchiao Fault, Tectonic subsidence, Active fault, Taiwan

Citation: Chen, C. T., J. C. Lee, Y. C. Chan, and C. Y. Lu, 2010: Growth normal faulting at the western edge of the Metropolitan Taipei Basin since the last glacial maximum, northern Taiwan. Terr. Atmos. Ocean. Sci., 21, 409-428, doi: 10.3319/TAO.2009.11.13.01(TH)

1. INTRODUCTION

History of fault development is often tape-recorded in syn-tectonic sediments associated with the fault motion. Such growth faulting scheme has been invoked to interpret fault slip accumulation over time and variation of strata across and along strike, leading to models describing fault evolution and kinematics (e.g., Childs et al. 2003; Bull et al. 2006). Much attention has been paid to growth strata genesis in compressional tectonic environments, such as foreland settings in determining fault-fold kinematics (Vergés et al. 2002; Hubert-Ferrari et al. 2007). Growth faulting along with sequence analyses were successfully applied to understand basin formation and petroleum systems in the northern Gulf of Mexico where deltaic shelf sediment infills are modulated by gravity-driven normal faulting and eustatic sea level change (Brown et al. 2004). Growth faulting may form at low elevations in the vicinity influ-

* *Corresponding author*
E-mail: jclee@earth.sinica.edu.tw

enced by recent sea level rise, and thus serve to be a potential tool for neotectonic investigations on seismogenic normal faults.

Normal fault system is one of the important sources of earthquake hazard in continental extensional provinces, where large plains, and therefore urban development and heavy populations, are often present. Examples of paleoseismology and earthquake geology studies in such setting include the Tyrnavos Basin in the Aegeon region (Caputo et al. 2004), the Wasatch Fault Zone in central Utah, United States (Machette et al. 1991; McCalpin and Nishenko 1996), and the upper Rhine Graben near Basel, northern Switzerland (Meghraoui et al. 2001). The Taipei metropolis, the capital of Taiwan where several million people reside, is unfortunately also under seismic threat from the active Shanchiao normal fault (Fig. 1; Chang et al. 1998; Lin et al. 2000). Since pioneering studies of the Shanchiao Fault (e.g., Lin 1957; Wu 1965), the geological characteristics of this fault have remained relatively poorly understood though they bear important information on hazard mitigation and regional geodynamics. Properties of the activity of the fault such as its long-term Quaternary slip rate are mostly inferred from geologic data in the Taipei Basin (Teng et al. 2001) and are therefore crude in nature. Recently, Huang et al. (2007) correlated the sediments of three borehole sets across the deduced fault surface trace (Lin 2001) and proposed three paleoseismic events during the Holocene; the validity of their analysis is doubtful as the borehole sets may have covered only part of the Shanchiao Fault zone when considering the geometry of the basin basement. In this study, we re-compiled their borehole set in the central part of the Shanchiao Fault to form the Wuku Profile (Fig. 2a). The stratigraphy of the three wells in the Wuku Profile is correlated and a geologic cross-section is thus revealed.

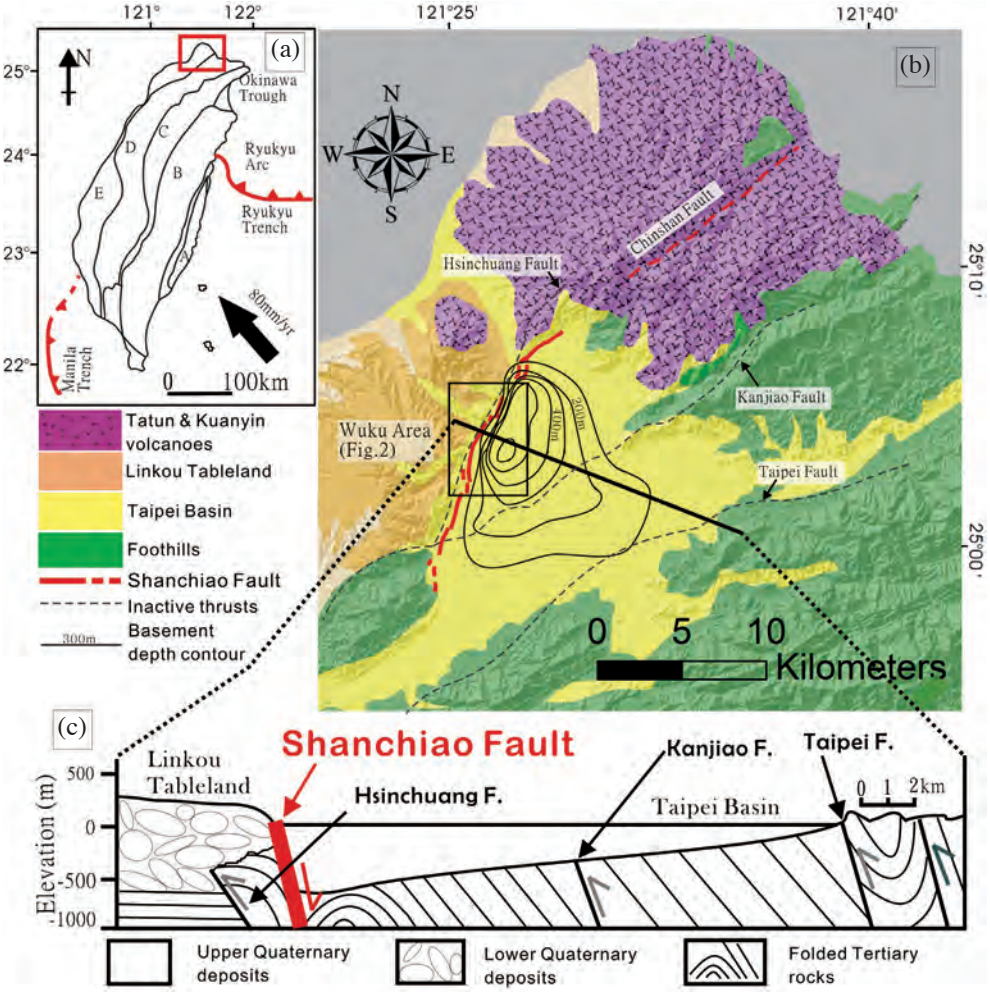

Fig. 1. (a) General tectonic framework of Taiwan. A: Coastal Range; B: Backbone Range; C: Hsueshan Range; D: Western Foothills; E: western Coastal Plain. (b) Simplified geology of the Taipei area. Four geological domains are defined in the Taipei area as indicated by different colors shown in the legend. The thick red lines are the Shanchiao Fault traces (Chen et al. 2006). Thin black lines within the Taipei Basin are the basement depth contour of 100 m interval (adapted from Teng et al. 2001). (c) Geological cross section of the Taipei Basin (modified from Teng et al. 1999).

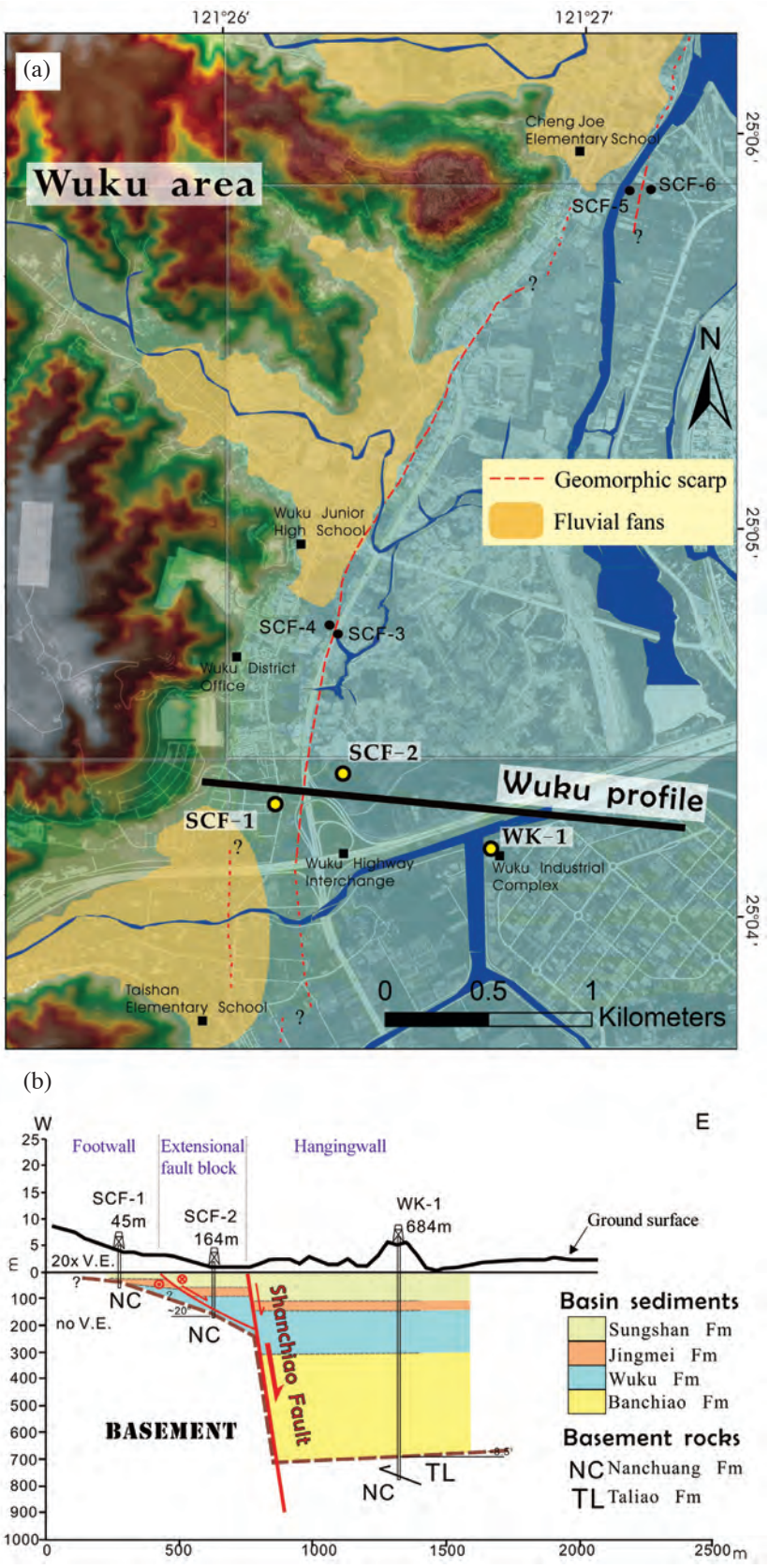

Fig. 2. (a) Map of the Wuku area, showing locations of the three boreholes used in this study, the Shanchiao Fault trace (dashed lines), and geomorphic features. (b) Interpreted Wuku geological profile. We interpret the Shanchiao fault as a combination of a main fault between SCF-2 and WK-1 to the east and the branch fault between the SCF-1 and SCF-2 to the west. Note that there is no vertical exaggeration beneath the sea level, and 20 times vertical exaggeration for surface topography.

In this paper, we document a valuable example of subaerial growth faulting case in the central portion of the Shanchiao Fault where growth strata provide a clear distinction on the sedimentation rate and throw rate across the fault on the thousand-year scale. A detailed growth faulting history is constructed over a time span since the Last Glacial Maximum revealing close coupling between sedimentation, tectonic process, drainage system changes, and eustatic sea level rise. Fault zone location and its deformation structure within unconsolidated basin sediment can therefore be better defined. Vertical slip rates on main and branch faults starting from 23 ka are constrained, implying an approximately 2 mm yr^{-1} averaged tectonic subsidence rate across the Shanchiao fault zone for the last 8400 years.

2. GEOLOGICAL SETTING

Taiwan is situated on the plate boundary of active convergence between the Eurasian and Philippine Sea plates since around 5 Ma (Suppe 1981; Ho 1986; Teng 1990; Wu et al. 1997) with a rapid convergence rate of about 82 mm yr^{-1} in the NW direction (Seno 1977; Yu et al. 1997; Lin et al. 2010; Fig. 1a). This oblique convergence leads to the southward-propagation of the Taiwan orogeny (Suppe 1981). Unlike regions of central and southern Taiwan presently in a state of full and mature collision (Angelier et al. 1986; Yu et al. 1997; Shyu et al. 2005), the northern part of the mountain belt, including the Taipei region, is now in a state of post-collision with an extensional or transtensional tectonic setting rather than a compressional one (Teng 1996), as evidenced by the presence of Quaternary extensional structures (Lee and Wang 1988; Lee 1989; Lu et al. 1995), extensional earthquake focal mechanisms (Yeh et al. 1991; Kao et al. 1998), and GPS displacement fields (Yu et al. 1997; Rau et al. 2008). The Taipei half-graben of Quaternary deposits is therefore formed in a close association with down-dip slips on the Shanchiao Fault, which is considered to be the major neotectonic structure responsible for the tectonic inversion from compression to extension across the Taipei region (Teng et al. 2001; Fig. 1).

The flat low-lying Taipei Basin, a triangular-shaped half-graben filled with late-Quaternary fluvial deposits since c. 400 ka (Wei et al. 1998; Teng et al. 2001), developed on top of the folded Oligo-Mio-Pliocene shallow marine strata, as a fold-and-thrust belt during earlier stage of mountain building. The late Quaternary terrestrial deposits in the Taipei basin form an asymmetric sedimentary wedge: reaching a maximum depth of about 700 m near the western margin and becoming thinner rather drastically toward the east and south (Fig. 1c). These unconsolidated deposits are divided into four major lithostratigraphic units (Teng et al. 1999). From bottom to top (Fig. 2b), they are: (1) the *Banchiao Formation*: consisting of intercalated fluvial sand, mud and conglomerate, with occasional pyroclastics and topped by thick laminated mud, with a maximum thickness of 380 m with ages ranging from 250 to 400 ka; (2) the *Wuku Formation*: consisting of fluvial sands and conglomerates, with minor mud and lateritic conglomerates, reaching a maximum thickness of c. 160 m with ages ranging from 80 to 250 ka; (3) the *Jingmei Formation*: comprising lateritic fluvial (alluvial-fan) conglomerates with an utmost thickness of 50 m. These particular conglomerate layers are interpreted as products when the Tahan River was captured and flowing into the Taipei basin about 25 to 23 ka (Teng et al. 2004a); (4) the *Sungshan Formation*: composed of estuarine interbedded sand-mud deposits, with a thickness of 50 - 100 m. The basin deposits are marked by prominent lateral facies changes with frequent pinch-outs. However, the widespread lateritic gravels of the Jingmei Formation and the laminated mud in the upper Banchiao Formation (Teng et al. 2004b) usually serve as basin-wide marker beds (Teng et al. 1999).

Geological evolution of the Taipei Basin was proposed by Teng et al. (2001), based on interpretation of regional geology. While the Plio-Pleistocene orogeny of mountain building reached its climax in northern Taiwan in Quaternary, the Paleo-Tanshui River, the major river in the Taipei Basin, began to provide sediments to produce the Linkou fan-delta around the ancient mountain front (Chen and Teng 1990). Accompanying the waning of compressive stress in the northernmost Taiwan island during the middle to late Quaternary (Lee and Wang 1988) is the vigorous eruptions of the Tatun volcanoes to the north of the Taipei Basin (Wang and Chen 1990; Song et al. 2000), probably reflecting the onset of regional extension. Subsidence along western margin of the Taipei basin, as evidenced by several hundred meters of thick fluvial deposits, is interpreted as a result from repeated normal faulting (the Shanchiao Fault) as inverted from the Hsinchuang fault, an ancient frontal thrust in northern Taiwan (Chiu 1968; Hsieh et al. 1992). The extension tectonics gradually transformed the Taipei area from rugged mountains into a sediment-receiving basin. The accumulation of fluvial and lacustrine sediments started at about 0.4 Ma (Wei et al. 1998; Teng et al. 2001). Since then the Taipei Basin has kept expanding due to erosion and continual asymmetric subsidence along the Shanchiao Fault in the western edge of the basin. Under the combining influences of sea level fluctuations, volcanic activities, drainage system changes, and tectonic processes, the basin was infilled with various types of sediments, including alluvial, lacustrine, marine and pyroclastic deposits, up to 700 m thick as mentioned above.

3. THE ACTIVE SHANCHIAO FAULT

The Shanchiao Fault was mapped (Lin 2001; Chen et al. 2004, 2006; Huang et al. 2007; Figs. 1b and 2a) along the topographic boundary between the Linkou Tableland and the Taipei Basin, sub-parallel to the Hsinchuang Fault (Lin

2001; Teng et al. 2001). There are features which indicate that the steeper Shanchiao normal fault may merge into the Hsinchuang thrust fault at depth (e.g., Hsieh et al. 1992). Following the late-Quaternary tectonic inversion, tectonic subsidence from down-dip slips on the Shanchiao Fault led to formation and development of the Taipei Basin. Left-lateral transcurrent motion together with clockwise block rotation is also expected to occur along the Shanchiao Fault, based on studies on regional structural geology, paleomagnetism, and GPS measurements (Lu et al. 1995; Lee et al. 1999; Rau et al. 2008).

Much effort has been made to characterize this active fault. Shallow reflection seismic profiling across the Shanchiao Fault imaged vertical offsets of Holocene sediments at shallow depths, although the location of the main fault remains questionable (Wang and Sun 1999; Shih et al. 2004). GPS surveys of the Taipei area showed WNW-ESE extension with a slow rate of 0.08 μstrain yr^{-1} across the fault (Yu et al. 1999). Asymmetric tectonic subsidence related to the Shanchiao Fault across the basin was illuminated through recent study on 30-year-long levelling data (Chen et al. 2007). Huang et al. (2007) correlated stratigraphy of three sets of boreholes, and proposed three paleoseismic events during the Holocene (i.e., at 8500, 9200, and 11100 years b.p., respectively). Geomorphology analysis also reveals a series of scarps closely related to the development of the Shanchiao Fault (Chen et al. 2006; Fig. 2a). Radon and helium anomalies in soil-gas along the fault zone were documented (Walia et al. 2005) indicating the presence of possible active faults and a deep fracture-advection system. The Shanchiao Fault is therefore considered currently active (Chang et al. 1998; Lin et al. 2000). Subsurface geology of the fault zone, by contrast, has not been fully explored.

4. RECONSTRUCTION OF GEOLOGICAL PROFILE ACROSS THE SHANCHIAO FAULT

In recent years, the Central Geological Survey of Taiwan carried out a number of drillings in the Taipei Basin in order to better understand its subsurface geology and engineering environment (e.g., Lin et al. 1999). Among them three boreholes in the Wuku area, SCF-1, 2, and WK-1, have been selected for the present analysis due to their optimal locations associated with the Shanchiao fault (Fig. 2a) and data quality. All three wells are situated in a flat marshy lowland in the Wuku area on the western edge of the basin. Drill hole WK-1 reaches the deepest known depth of the late Quaternary basin deposits at 679 m. Many radiocarbon dates have been acquired (Lin et al. 1999) which are crucial for a successful stratigraphic correlation. At SCF-1 and SCF-2 boreholes, the Sungshan Formation in the upper part was studied by Huang et al. (2007) whose classification of strata serves as a basis for this study. The main stratigraphic system of the complete basin deposit is adapted from Teng et al. (1999), as discussed above. Through stratigraphic analysis of the three boreholes by incorporating the growth faulting scheme, we reconstruct the Wuku geological profile to reveal the present configuration of fault zone stratigraphy and structure in the central part of the Shanchiao Fault.

4.1 Stratigraphic Correlation between the Boreholes

First, we carried out analysis and correlation of stratigraphic units between the three boreholes, SCF-1, SCF-2 and WK-1, based on lithology and radiocarbon dates. We reprocessed all available raw radiocarbon dates previously published (Lin et al. 1999; Huang et al. 2007) by calibrating these radiocarbon dates to calendar years before present (cal. yr BP) using the model curve of Fairbanks et al. (2005). Table 1 shows details of the results. Note that a few calibrated radiocarbon dates reveal a reversed stratigraphic order (i.e., older ages on top of younger ones), implying that they might be reworked samples. Thermoluminescence ages acquired in WK-1 (Lin et al. 1999) are summarized in Table 2. We thus reconstructed a detailed correlation of lithostratigraphic units of the three boreholes (Fig. 3) and the unit descriptions are listed in Table 3. Comparing the strata in three boreholes (SCF-1, SCF-2, and WK-1), one finds that the thickness of all the four formations increases dramatically toward the east. Hereafter we describe how we correlated the lithofacies units between these three boreholes (Fig. 3).

For the uppermost Sungshan Formation at SCF-1 and SCF-2, Huang et al. (2007) divided this formation into three units as C1, C2, and C3. We find that such division also applies to the Sungshan Formation at WK-1 (Fig. 3 and Table 3). The C1 unit is comprised of mainly sandy layers with mollusk shells at bottom whose onset of deposition is around 8400 years B.P. (8.4 ka) and is of alluvial facies (Huang et al. 2007). At SCF-1 this unit extends from land surface to a depth of 14.5 m (where the shells occur) and is filled with fine to medium sand with occasional thin silts at 2 - 3 and 8 m depths. At SCF-2 this unit is composed of fine sands with one thin mud and silt layer and ends at the shell lag of 22.3 m in depth. Collectively, we find that the C1 unit shows a prograde depositional character in both SCF-1 and SCF-2. At WK-1 the shell layer is found at 33.6 m with an age ~8.4 ka, which lies under interlayers of fine to medium sands and muddy-silts; these sediments of floodplain facies in a prograding fashion (Teng et al. 2000) are therefore considered to be correlative to the C1 unit.

Underneath the C1 unit, the C2 unit which was deposited from ~9 to 8.4 ka is predominantly clayey and rich in peat and charcoal as defined at SCF-1 and SCF-2 (Huang et al. 2007). The upper part of C2 at SCF-1 is filled with muddy silts and the lower part with mud to a depth of 21.3 m. At SCF-2 the C2 unit consists of mud in the upper section

Table 1. Radiocarbon age data of the three boreholes along the Wuku Profile.

Borehole	Data source*	^{14}C age (yr B.P. ± 1σ)	Calendar year range** (cal. yr B.P.)	Depth (m)	Unit
SCF-1	(1)	5730 ± 40	6457 - 6567	5.35	C1
	(1)	5697 ± 46	6418 - 6528	9.40	C1
	(1)	7590 ± 130	8280 - 8506	16.12	C2
	(1)	7923 ± 58	8618 - 8868	22.80	C3
	(1)	8450 ± 120	9345 - 9563	32.30	C3
	(1)	8620 ± 60	9517 - 9611	34.99	C3
SCF-2	(1)	5625 ± 49	6348 - 6450	10.40 - 10.50	C1
	(1)	7635 ± 55	8381 - 8463	19.20 - 19.30	C1
	(1)	8018 ± 54	8834 - 9032	22.55	C2
	(1)	7790 ± 50	8518 - 8612	30.40	C2
	(1)	8200 ± 56	9057 - 9239	36.70	C3
	(1)	8400 ± 160	9223 - 9567	49.00	C3
	(1)	9064 ± 67	11176 - 11270	55.50	C3
	(1)	34060 ± 600	38824 - 40038	87.52	Jingmei
	(1)	> 50000	N/A	102.20	Wuku
	(1)	> 47100	N/A	138.18	Wuku
WK-1	(2)	7160 ± 70	7917 - 8037	24.80	C1
	(2)	7560 ± 70	8321 - 8425	36.55	C2
	(2)	7930 ± 60	8628 - 8888	42.2 - 42.6	C2
	(2)	9010 ± 110	10035 - 10301	49.4 - 50.2	C2
	(2)	8660 ± 80	9515 - 9705	50.2 - 50.4	C2
	(2)	9090 ± 60	10196 - 10280	54.7 - 55.05	C3
	(2)	10180 ± 150	11549 - 12151	63.4 - 63.8	C3
	(2)	9530 ± 60	10687 - 10967	67.6 - 67.7	C3
	(2)	10080 ± 60	11493 - 11805	68.6 - 68.7	C3
	(2)	9810 ± 80	11159 - 11285	74.1 - 74.7	C3
	(2)	18950 ± 540	21914 - 23228	89.3 - 89.5	C3
	(2)	21300 ± 160	25287 - 25777	94.0 - 94.1	C3
	(2)	> 42000	N/A	183.6	Wuku
	(2)	> 50000	N/A	219.3	Wuku

** Raw radiocarbon ages: (1) Huang et al. 2007 and (2) Lin et al. 1999; ** Calibration with Fairbanks 0107 calibration curve (Fairbanks et al. 2005); N/A = not available.*

Table 2. Thermal luminescence (TL) ages. Data from Lin et al. 1999.

Borehole	TL age	Depth (m)	Unit
WK-1	80 - 120 ka	155.9	Wuku
	83 - 113 ka	177	Wuku
	73 - 99 ka	234.2	Wuku
	164 - 264 ka	251	Wuku
	169 - 227 ka	328	Banchiao
	192 - 288 ka	351.5	Banchiao

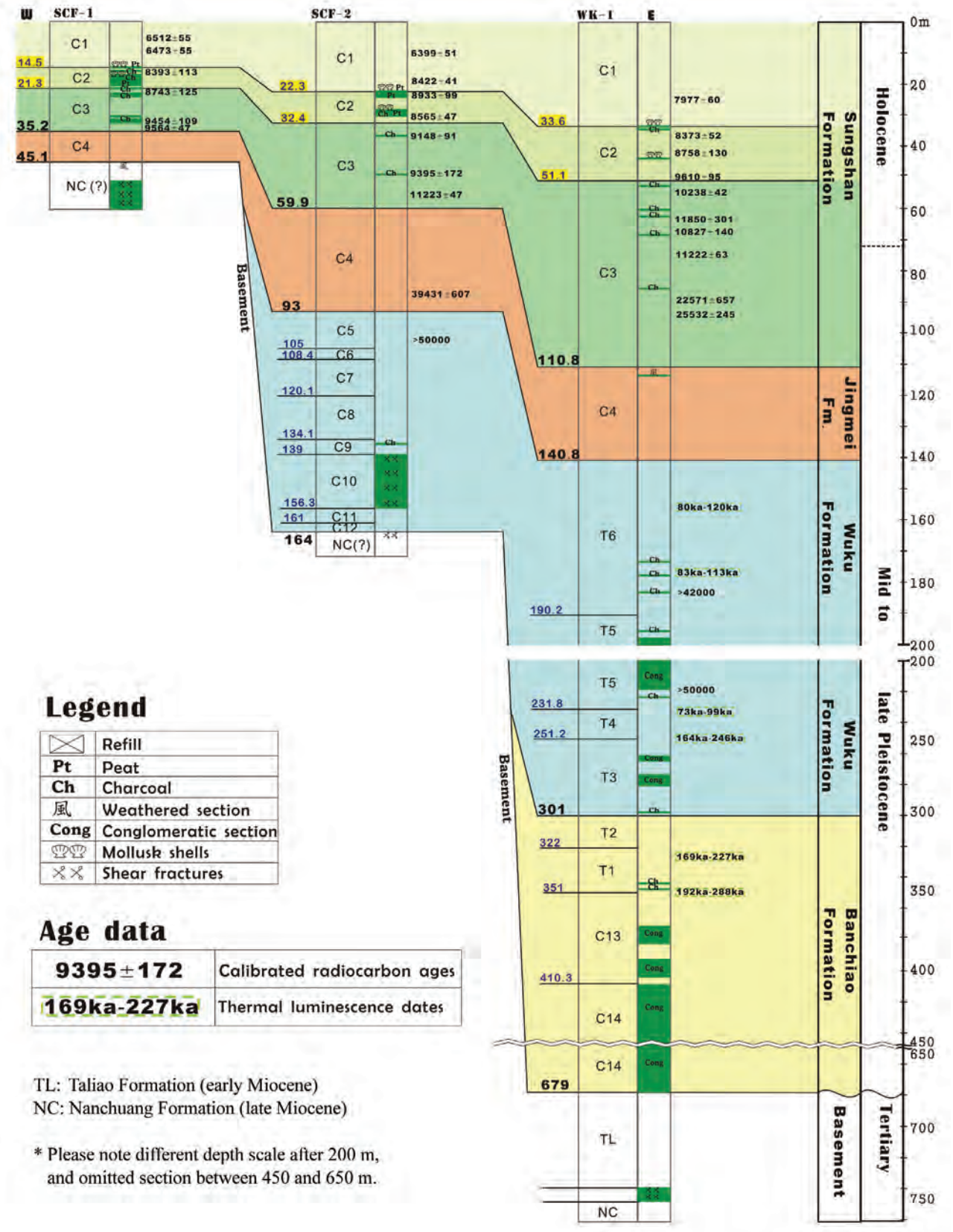

Fig. 3. Stratigraphic correlation between boreholes (SCF-1, SCF-2, and WK-1) of the Wuku profile. Location of the boreholes is indicated in Fig. 2. Four major geological formations consist of the late Quaternary deposits of the Taipei basin: from top to bottom, the Sungshan, Jingmei, Wuku, and Banchiao Formations. Each formation has been divided into several stratigraphic units. See details in the text. Please note different depth scales between 0 - 200 and 200 - 750 m, and omitted section between 450 and 650 m.

Table 3. Lithofacies of the Wuku Profile.

Unit	Description	Thickness (m)			Stratigraphy*	Reference**
		SCF-1	SCF-2	WK-1		
C1	Mainly sandy layers, parallel lamination in clayey layers, mollusk shells at bottom	14.5	22.3	33.6	Sungshan	a
C2	Mainly clay layers, occurrences of mollusk shells, peat in top section, paleosol and peat in middle section, charcoal-rich bottom section	6.8	10.1	17.5	Sungshan	a
C3	Sand within thin charcoal-rich clay layers, occurrences of paleosols	13.9	27.5	59.7	Sungshan	a
C4	Lateritic conglomerates with minor grey gravels	9.9	33.1	30	Jingmei	b
C5	Brown-grey silty sand	-	12	-	Wuku	This study
C6	Conglomerate with grey silt	-	3.4	-	Wuku	This study
C7	Brown silt	-	11.7	-	Wuku	This study
C8	Conglomerate with brown clay	-	14	-	Wuku	This study
C9	Charcoal-rich silt	-	4.9	-	Wuku	This study
C10	Sand-silt thin interlayers (containing several sheared sections localized in silt layers)	-	17.3	-	Wuku	This study
C11	(Tuffaceous?) silt	-	4.7	-	Wuku	This study
C12	Conglomerate with yellow-brown clay	-	3	-	Wuku	This study
T6	Clay within thin silt/sand	-	-	49.4	Wuku	c
T5	Conglomerate bounded by sand	-	-	41.6	Wuku	c
T4	Non-stratified clay with sand of parallel and cross lamina	-	-	19.4	Wuku	c
T3	Two conglomeratic layers in sands	-	-	49.8	Wuku	c
T2	Varve with rare thin silt/sand	-	-	21	Banchiao	c
T1	Non-stratified clay containing vivianite concretes, cross-laminated sand at bottom section	-	-	29	Banchiao	c
C13	Silt-clay with thin conglomerates	-	-	59.3	Banchiao	This study
C14	Conglomerate with rare thin sand/silt	-	-	268.7	Banchiao	This study

** Defined in Teng et al. (1999); ** Reference for unit definitions: a: Huang (2003) and Huang et al. (2007); b: Teng et al. (1999); c: Teng et al. (1993).*

and silts near the bottom at 32.4 m. At WK-1 a thick muddy-silt layer of estuarine environment (Teng et al. 2000) extending to 51.1 m is found corresponding to the C2 unit with analogous sediments. In fact, the radiocarbon ages also support this correlation of stratigraphy. The sediments of the C2 unit are distinctively finer-grained than those above (C1 unit) or beneath (C3 unit), making it much easier to recognize. Abundant detrital charcoal chips and mollusk shells are present in C2 unit at all three boreholes.

The C3 unit, the lowermost member in the Sungshan Formation, is made up of sandy layers with alternating thin charcoal-rich clay layers older than 9 ka at SCF-1 and SCF-2. At SCF-1, the C3 unit consists of silts and fine sands 13.9 m thick wherein their accumulation started at ~10 ka. At SCF-2 the C3 unit is 27.5 m thick composed of interbedded fine sands and silts, and began sedimentation ~12 ka. Between 51.1 and 110.8 m depth at WK-1, alternating charcoal-rich layers of fine-medium sands and mud is found equivalent to the C3 unit described above, albeit of greater thickness and longer time span of deposition ranging from ~23 to ~9 ka. The C3 sediments in WK-1 exhibit an upward transition from alluvial fan to distal floodplain facies in a retrograde stacking pattern, without a break of sedimentation between C3 and underlying Jingmei Formation of C4 unit (Teng et al. 2000). By contrast, there appears a substantial hiatus at the same stratigraphic boundary between C3 and C4 units at

SCF-1 and SCF-2, according to the radiocarbon dates.

The Jingmei Formation (lateritic clast-supported conglomerate layer, C4 unit in Table 3) also appears to increase in thickness towards the east. At borehole SCF-1, it rests unconformably above weathered Tertiary basement rock and is 9.9 m thick. At SCF-2 it is 33.1 m thick (between 59.9 to 93 m), and at WK-1 it is 30 m (between 110.8 to 140.8 m), both lying on the Wuku Formation. The Jingmei Formation, a product from the diversion of the Tahan River into the Taipei Basin, was interpreted to be formed during 23 and 25 ka (Teng et al. 2004a). The only radiocarbon date of 38 - 40 ka in the lower part of the Jingmei Formation at SCF-2 is presumably acquired from reworked material.

The remaining lower part of SCF-2 of about 71 m thick (93 - 164 m), below the Jingmei Formation, is composed of silts in combination of sands, with three conglomeratic units, and is defined as the upper part of the Wuku Formation (C5 - C12 units), which lies unconformably upon the folded Miocene basement rocks. At borehole WK-1, below the Jingmei Formation, two late Quaternary formations lying unconformably above the Tertiary basement rocks can be observed: (a) the Wuku Formation lies in between 140.8 to 301 m (about 140 m thick) and (b) the underlying Banchiao Formation extends from 301 to 679 m (378 m thick). The uppermost Wuku Formation was dated to be far older than 50 ka, implying a large gap of sedimentation before the onset of depositing the overlying Jingmei conglomerates. The oldest dated age for the Wuku Formation is about 200 ka at WK-1 borehole. The Banchiao Formation constitutes the lower half of the WK-1 borehole. Existing thermoluminescence ages imply that the age for the Banchiao Formation is no younger than 150 ka (Table 2) and might be no older than 400 ka (Wei et al. 1998; Teng et al. 2001).

All three boreholes penetrated to the Tertiary basement rocks which are known exposed surrounding the Taipei Basin as the rugged foothills. Basement rocks reached at SCF-1 and 2 are probably the late-Miocene Nanchuang Formation, with weathered top basement rock in SCF-1. Rocks retrieved from WK-1 in 679 to 741 m belong to the early Miocene Taliao Formation, which is thrust over the Nanchuang Formation at 750 - 760 m depth by a shear zone containing fault breccias (Lin 2005). Note the dramatic increase of basement depth between SCF-2 and WK-1 boreholes compared to a relatively mild one between SCF-1 and SCF-2 boreholes (Fig. 2b), implying the location of the main Shanchiao Fault between the SCF-2 and WK-1 and will be discussed later in more detail.

Through lithologic correlation in aid of radiocarbon ages, the Sungshan and Jingmei formations are present across the entire profile, while the Wuku Formation is only found at SCF-2 and WK-1, and the Banchiao Formation is restricted to WK-1. The Sungshan Formation (and units within), the Jingmei Formation, and the Wuku Formation all thicken toward the east, and the stratigraphic horizons deepen eastward. The sedimentation rate appears to vary both temporally and spatially. We found two major hiatus: one between the deposition of Wuku and Jingmei sediments and the other between the deposition of the Jingmei and Sungshan sediments at SCF-1 and 2. Sediments within the Sungshan and Jingmei formations are quite similar between the boreholes, indicating the sediment source was generally the same and was presumably basin wide, as from the Tahan - Tanshui river system (sediment transporting direction normal to the profile and rather homogeneous). Tributaries drained from the Linkou Tableland to the east didn't seem to assert significant contribution to the deposits since no alluvial-fan conglomerates are found beyond the deposition of the Jingmei gravels in these boreholes suggesting little local sediment transport.

4.2 Stratigraphic Architecture of the Shanchiao Fault Zone

In active extensional settings, such as the Shanchiao fault area, the rate of increase of accommodation space is enhanced on the hanging-wall due to subsidence caused by normal faulting. Hereafter we briefly describe the theory of reconstructing the growth strata across an active normal fault we apply in this study. On a relatively flat depositional surface, sediments deposited within a given time span (growth strata) will be thicker on the hanging wall than those in the footwall if the normal fault is active, and uniform if there's quiescence in tectonic activity. The top of such layers will be even when deposition smooth out the fault scarp (if there is any), mimicking the regional topography. Subsequent layers will continue to form above the newly-formed horizon and repeat the geometric pattern governed by fault activity should there be room for sedimentation. Existing growth strata will be displaced downward at the same time and record all successive deformations. The entire package of syn-tectonic sediments may therefore yield information on fault location and structure, faulting history, and kinematics of fault-related folding (e.g., Sharp et al. 2000).

Based upon the above established stratigraphic correlation, the growth normal faulting scheme within shallow sediments are illuminated. First, architecture of the latest Sungshan Formation is most useful for its completeness and synchroneity of sedimentary facies within the Holocene time. Between the SCF-1 and SCF-2, the units within the Sungshan Formation are indeed down-thrown and thicken eastward, representing effects of normal faulting, as Huang et al. (2007) previously proposed, at the same site of mapped fault-related scarp by Chen et al. (2004). However, these effects on growth strata appear to be much more pronounced between boreholes WK-1 and SCF-2. We thus estimate the accumulation (sedimentation) rates at each drilling hole for the Sungshan Formation, including the C1, C2, and C3 units. By adopting the dated ages and the thickness of the units in

each hole with simple mathematics, we obtain a variation of thickness for each unit across the three holes (Fig. 4). It reveals that the thickness shows an eastward increasing trend for each unit, in particular across the SCF-2 and the WK-1 holes. As a result, the variations indicate the presence of a likely normal fault between SCF-1 and SCF-2 and a more significant vertical offset of normal faulting between SCF-2 and WK-1. We therefore intend to map two fault zones in the shallow sediments of the Wuku profile, with the eastern one as the main fault zone (Fig. 2b).

Because the interface between unconsolidated basin sediments and the Tertiary basement rocks dramatically deepens between boreholes SCF-2 and WK-1 to be at least 34° dip angle (Fig. 2b), we tend to interpret the main fault zone in further depth to follow this interface. The secondary fault zone between SCF-1 and 2 is supported by a shear zone near the bottom of the basin sediments at SCF-2 within the C10 unit, which contains several sheared intervals with striations denoting oblique sinistral-normal faulting and frequent centimeter-scale growth normal faults (Lee et al. 1999). This secondary fault may merge with the main fault zone at where the basement floor abruptly steepened. The secondary fault is therefore regarded as a branch fault, which develops within the basin sediments. We interpret the region between the branch and main fault zones as an 'extensional fault block.' The Wuku formation is much thinner in the extensional fault block than in the actual hanging wall east of the main fault zone, and probably a slim sheet of it remains west of the branch fault but is terminated east of SCF-1. The Banchiao formation is exclusively confined in the hanging wall in greater depth.

Figure 2b shows the proposed fault zone structure in the late-Quaternary basin sediments consisting of a high-angle main fault and a western lower-angle branch fault. Seismic profiling about 1.5 km south of the studied boreholes (Wang and Sun 1999) reveals similar two-fault setting in the Shanchiao Fault zone. Minor sinistral slip component is present on the branch fault according to oblique fault striations documented by Lee et al. (1999), and such fault zone configuration may genetically bear resemblance to a negative flower structure or tulip structure (Woodcock and Schubert 1994) as unveiled in a shallow seismic survey along the fault zone in the northern corner of the Taipei Basin (Shih et al. 2004).

We can not rule out the possibility that the branch fault zone between SCF-1 and 2 may extend down into the basement other than lying entirely within loose sediments. The extensional fault block may include the basement rock, producing staircase-shaped basement floor geometry in imbricate listric normal faulting (e.g., Wernicke and Burchfiel 1982). It is also possible that the area between SCF-1 and WK-1 rests above an extensional fault-propagation fold (e.g., Gawthorpe and Hardy 2002) with the two fault zones as trishear zone boundaries where shearing is concentrated. These options, though cannot be excluded, are not incorporated in the present study due to lack of evidence, and will not lead to momentous defects in the following presentation.

5. RECONSTRUCTION OF GROWTH FAULTING HISTORY

5.1 Sea Level Fluctuation and Sedimentation in the Taipei Basin

Sedimentary processes in coastal areas and their vicinities are sensitive to base level changes (van Wagoner et al. 1988), so are in the Taipei Basin. Teng et al. (2000) noted two erosion surfaces below lowstand systems tracts in the basin deposits. Sedimentary facies of the basin deposits include estuary and lake, distal to proximal floodplain, braid plain, and alluvial fan facies (Peng et al. 1999; Teng et al. 2000). Given that the present sits at the highstand of the eustatic sea level cycle since around 20 ka of the Last Glacial Maximum (LGM)(Fig. 5), the youngest basin deposits of the Sungshan Formation (10 - 23 ka to present) were accumulated during the recent sea level rise. Before the Jingmei conglomerates deposited at about 25 ka when the Tahan River was captured, the basin (by then covered by the Wuku Formation) was in a stage of erosion with deeply-incised valleys (Teng et al. 2000, 2004a) during the period of LGM. The restored geometry of the top of the Wuku formation represents the paleogeography of the Taipei Basin in LGM. Subsequent stacking of Jingmei and Sungshan deposits, belonging to the most recent sequence, can be discerned by linking rates and facies of sedimentation to accommodation provided by base level rise and tectonic subsidence.

Under the basin-wide deposition scheme described above, the geological history of the sediments in association with the activity of the Shanchiao Fault since the LGM can be illuminated through sedimentary records recovered from the investigated boreholes. A series of retro-deformed cross-sections can therefore be established since LGM of about 25 ka. In the following two sections, we first present the criteria for generating the restored cross-sections by a back-stripping method and the resultant profiles, and then illustrate the geological evolution of the Shanchiao Fault zone starting from 25 ka through semi-quantitative sections under the same scheme. Compaction of loose sediments is negligible because of the young ages and shallow depths of the units (Chen et al. 2007; Taylor et al. 2008).

5.2 Restoration by a Simple Back-Stripping Method

As mentioned above, the basin-wide sedimentation process in late Quaternary was governed by sea level fluctuations along with changes of drainage system, so did the accumulation of Sungshan and Jingmei Formations in the Wuku Profile since local influences other than tectonics

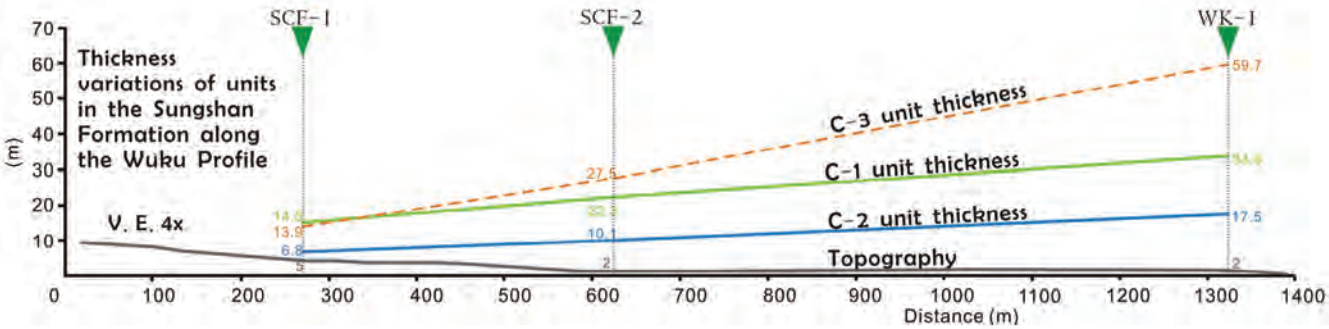

Fig. 4. Thickness variations of units in the Sungshan Formation along the Wuku Profile. Three units all show an increase of thickness toward the east, strongly suggesting growth faulting in-between the drilling holes. By comparing the present topography, the thickness variations clearly exceed differences of local topography and therefore advocate syn-sedimentation normal faulting.

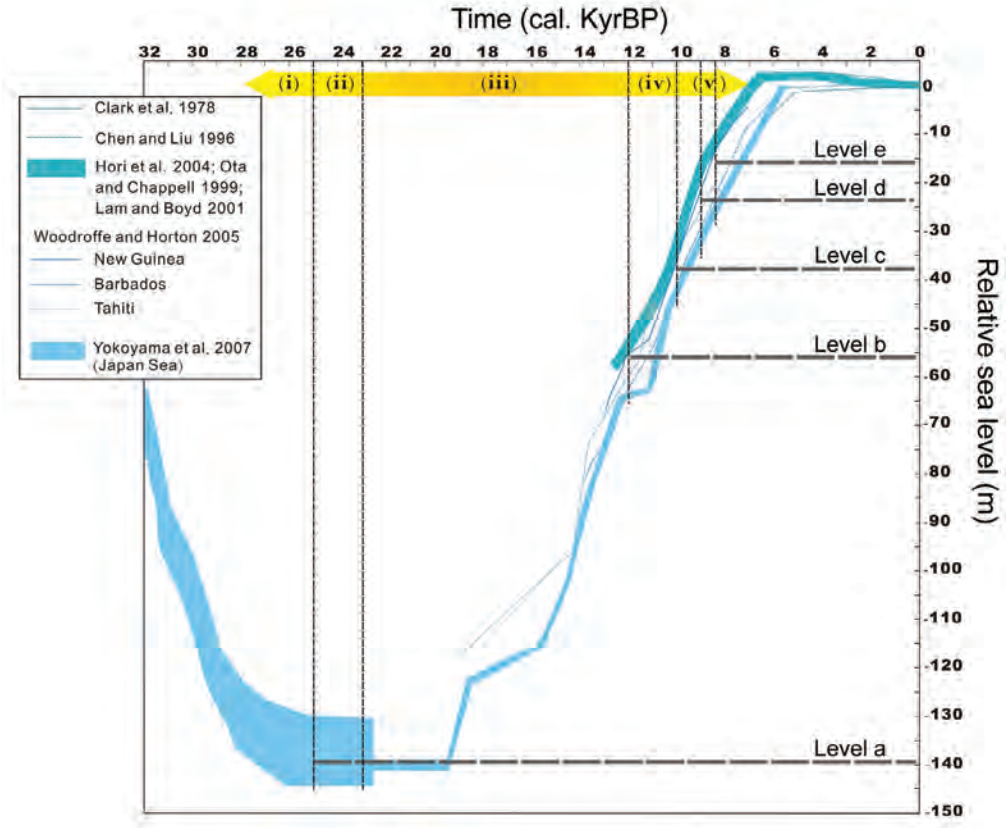

Fig. 5. Eustatic sea level changes since 30 ka. Levels are compiled from Clark et al. 1978; Chen and Liu 1996; Ota and Chappell 1999; Lam and Boyd 2001; Hori et al. 2004; Woodroffe and Horton 2005; and Yokoyama et al. 2007. In addition to the present-day sea level, five paleo-levels (Level a - e) were selected as the sea levels corresponding to specific ages with significant geological processes. See details in the text.

are not observed in sediment records. When the sea level reached similar elevation to that of the Taipei Basin plain (resembling the present configuration) since the recent major marine incursion in the basin at 10 - 9 ka (Teng et al. 2000), sediments piled up across the entire profile, including the footwall, hanging wall and extensional fault block areas. Given the high rate of erosion and hence rapid sediment accumulation of the Taiwan Island in the present day (Dadson et al. 2003), the room of sedimentation created by rising eustacy is considered to be filled up contemporaneously, therefore producing flat topography similar to the modern one.

Under this assumption, the topography at beginning of the deposition for the C1 unit of the Sungshan Formation would be approximately flat. Because the C1 unit of SCF-1 lies in the footwall area, hence it would not involve significant vertical motion of the faulting. Referring to the growth normal faulting scheme, the bases of C1 units in the hang-

ing wall side would be expected to be consequently downward displaced by dip-slips of the Shanchiao Fault which provided additional sedimentation rooms resulting in lateral thickening of the units. The elevation differences between the base of C1 unit at SCF-2 and SCF-1 (7.8 m), and SCF-2 and WK-1 (11.3 m) thus are interpreted to represent cumulative vertical displacements on the branch and main faults, respectively, from 8.4 ka till present (Fig. 6a). Furthermore, we can observe that the height of sea level e (around -16 m) at the onset of the C1 (~ 8.4 ka) is close to the depth of the base of the C1 unit (-14.5 m) in the footwall area (SCF-1).

Back to 8.4 ka, because that the top of the basin deposits (C2 unit) in the footwall appears to be near the sea level (level e), therefore the height of the top of the estuarine deposits of the C2 unit across the profile would be considered to be very much flat. Under this assumption, the fault zone stratigraphic configuration by then can be approximated by removing the C1 unit above and re-leveling the C2 unit tops in WK-1 (hanging-wall region) and SCF-2 (extension fault block) to the one at SCF-1 (footwall region) as restoration by 'back-stripping' (Fig. 6b). We calculate the remaining vertical differences of the depths of C2 unit between three holes as mentioned above. We then obtain 3.3 and 7.4 m, which hence denote to be cumulative vertical offsets on the

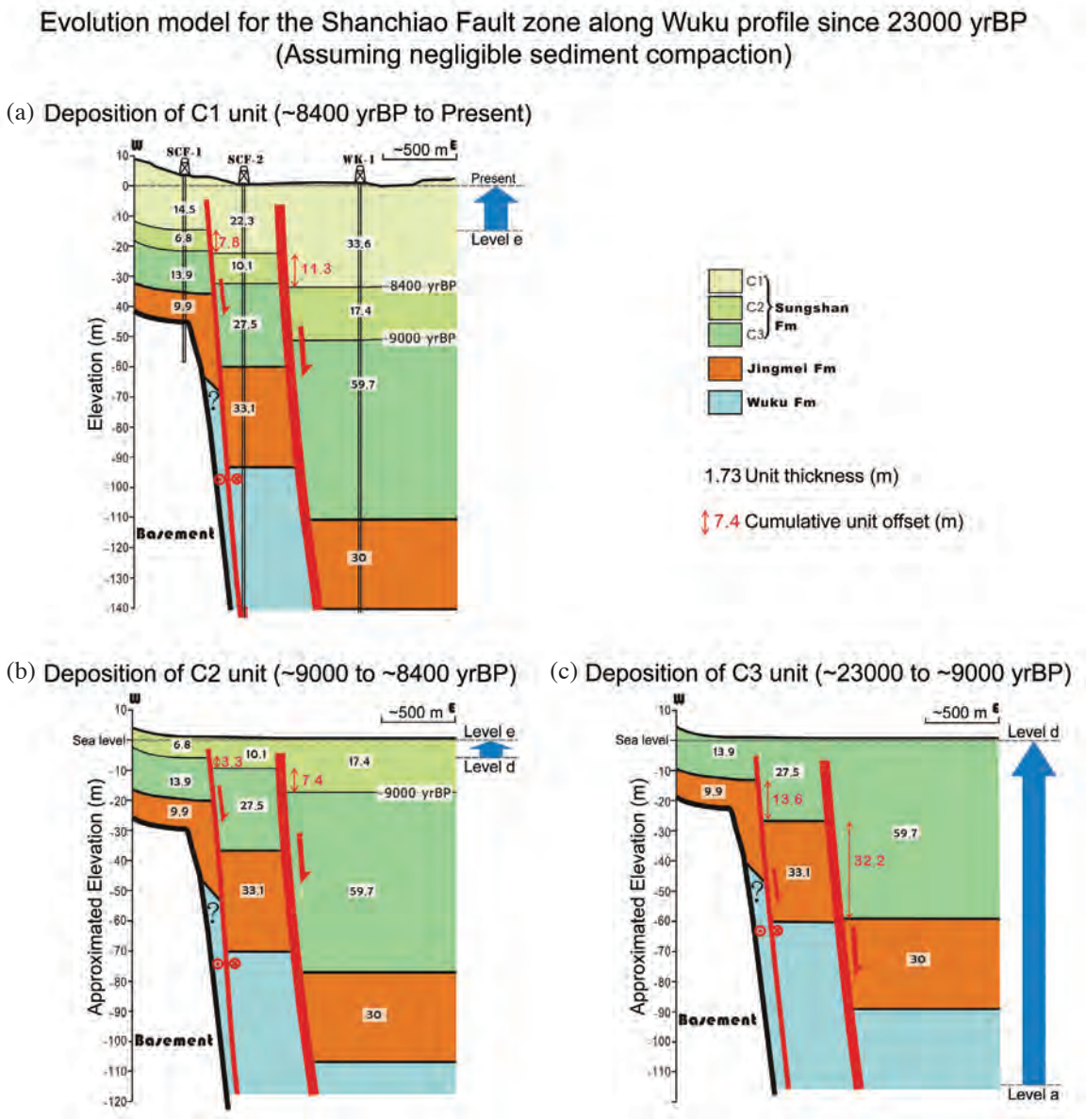

Fig. 6. Back-stripping method and reconstruction of cumulative deformation on the Shanchiao Fault since the LGM of about 23 ka. Three periods of 8.4 ka - present (a), 9 - 8.4 ka (b), and 23 - 9 ka (c), which correspond to depositional ages of Units C1, C2, and C3, respectively, are adopted for explaining the evolution of the growth faulting of the Shanchiao Fault. Numbers in black color: thickness of stratigraphic units. Numbers in red: vertical differences of thickness for each stratigraphic unit between drilling holes. Levels a to e are paleo-sea levels through time, which are denoted in Fig. 5.

branch and main faults respectively during the 9 to 8.4 ka period (Fig. 6b). These relatively large amounts of vertical offset in a short time span of 600 years appear to be consistent with two possible earthquake events occurred during this period inferred by previous study (Huang et al. 2007). We will discuss it in more detail in the later section.

The above approach became much difficult to apply to deeper sediments of the Sungshan Formation because the 10 ka datum is obscure at SCF-2 and WK-1, and synchroneity of sedimentation along the Wuku profile was absent during 23 to 10 ka. However, the Jingmei Formation alluvial fan deposits of 25 - 23 ka resulted in a relatively flat topography at the end of the river-capture event. Provided the comparable thicknesses of the Jingmei conglomerates (C4 unit) at SCF-2 and WK-1, the ancient topography of the Wuku profile is considered to be roughly even at around 23 ka, therefore permitting the 'back-stripping' of C3 unit and evaluation of fault vertical displacements during the deposition of the C3 unit. Under this assumption, we then obtain that the Shanchiao branch fault slipped 13.6 m vertically and the main fault 32.2 m during ~23 ka to 9 ka according to constraints from top horizons of the C3 unit and the Jingmei Formation (Fig. 6c).

Details of sediment accumulation and fault throws between ~23 to 9 ka cannot be accurately resolved, while the stacking pattern of the deposits does show westward onlapping of layers which is closely tied to tectonic modification on local geomorphology and base level changes controlled by eustacy. Regional sedimentation rate (modulated by tectonic movements) was zero at the LGM as the sea level (level a) was low at about -140 m compared to the present day level. Since LGM the sedimentation rate is expected to be rapidly increasing in pace with the rising sea level, and again dropped to trivial numbers when eustacy stabilized to elevations similar to that of today at ~6 ka (Fig. 5).

In summary, the total vertical offset across the Shanchiao fault zones since 23 ka can be yielded by summing the above results during different periods, as shown in Fig. 6. We thus obtain a total vertical offset of 75.6 m, with 24.7 and 50.9 m for the branch fault and the main fault, respectively, since the LGM of 23 ka. It can translate to an average vertical fault slip rate of 3.3 mm yr^{-1} across the Shanchiao fault zone in Wuku profile, with 1.1 mm yr^{-1} for the branch fault and 2.2 mm yr^{-1} for the main fault, since 23 ka.

5.3 Evolution of Sedimentation vs. Growth Faulting

Combining information on stratigraphic architecture and knowledge on sea level changes since the LGM, the fault zone evolution is depicted in six scenes shown in Fig. 7.

(1) Shortly before 25 ka (Fig. 7a)

Global and East Asian eustatic sea level plunged to more than 100 m below the present level since 30 ka, as the LGM began (Yokoyama et al. 2007). The sea level around Taiwan stabilized at approximately -140 m (level a) from about 28 ka compared to the present day. The 25-ka paleotopography as top of the Wuku formation can be estimated by adding the present day -140.8 m deep with 75.6 m of total vertical subsidence due to faulting with our back-stripping method, as described above. We obtain a depth roughly at -65 m for the top of Wuku formation along the Wuku profile (Fig. 7a). It means that the Wuku formation was about 75 m high above the sea level at that time. As a result, sediments of the Wuku formation were subject to strong erosion by drainage system in the Taipei basin.

The relatively high local topography 75 m above sea level indicates that no major channels, neither the Tanshui River nor the creeks originated from the Linkou Tableland in the west, existed in the investigated profile, which would form gorge-like incised valleys. The shallow basement at SCF-1 was exposed without cover of late-Quaternary deposits and thus was subject to be weathered (Fig. 7a). Surface scarps resulted from slips on the Shanchiao Fault were likely to be rapidly erased or retreated westward on topography by intense erosion, obscuring attempts to estimate fault activity during this period.

(2) 25 to 23 ka (Fig. 7b)

The Jingmei sediments were interpreted to be quickly deposited when the Tahan River was captured into the Taipei Basin during 25 - 23 ka (Teng et al. 2004a). These alluvial fan conglomerates accumulated within a time span of 2000 year and attained ~30 m thick in the Wuku region. The top of the Jingmei conglomerates should be rather flat by the time deposition ceased in the Wuku Profile because sediment transport was normal to the profile towards the north and no major channels were present. The gravel bed of the Jingmei Formation is 10 m thick onlapping onto the weathered Mio-Pliocene basement at SCF-1, implying an ancient topographic scarp located between SCF-1 and SCF-2. However, we interpret that the Shanchiao Fault was inactive during this 2000-year-long period because the Jingmei Formation is of uniform thicknesses (i.e., 30 - 33 m) across the main fault between SCF-2 and WK-1.

On the other hand, during 25 to 23 ka, the sea level did not change significantly and remained about -140 m compared to the present level. So that the top of the Jingmei formation lies about -35 m compared to the present, that is, about 105 m high above the sea level.

(3) 23 to ~12 ka (Fig. 7c)

We anticipate that the Taipei basin started to subside along the Shanchiao Fault after completion of the Jingmei conglomerate with probably both the hanging-wall block and the extensional fault block displaced downward. However, braid plain to floodplain sediments of 23-12 ka (lower part of C3 Unit of the Sungshan Formation) exist only at

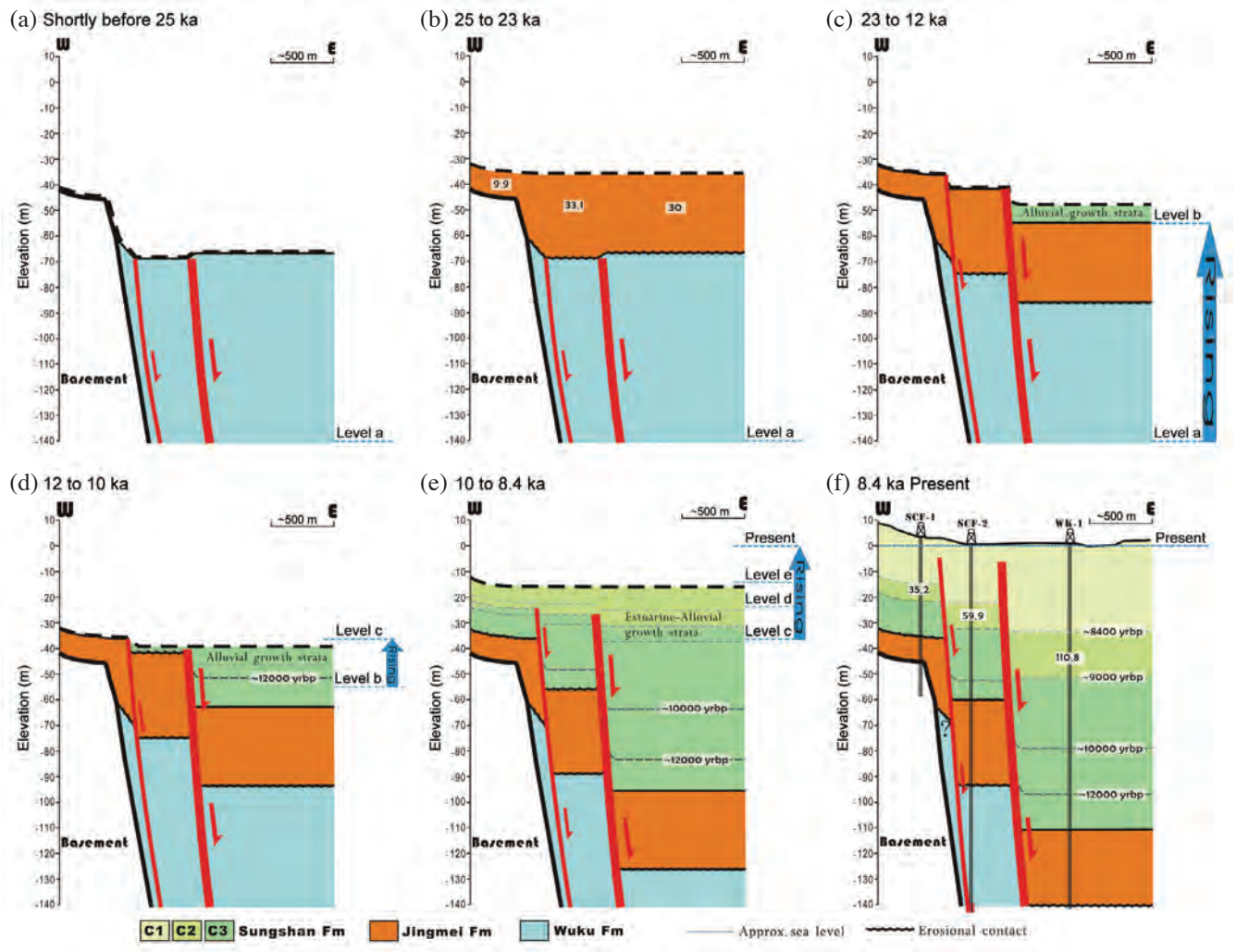

Fig. 7. Interpreted sedimentation and growth faulting and post-LGM development history of the Shanchiao Fault zone in the Wuku profile. Several geological events with confident age control were adopted to divide the period into six stages: (a) shortly before the deposition of the Jingmei formation (25 ka), (b) deposition of the Jingmei conglomerates (25 - 23 ka), (c) shortly before the sea level rising to reach the basin ground level (23 - 12 ka), (d) the sea level beginning to surpass the basin ground level (12 - 10 ka), (e) basin-wide sedimentation containing a 600-year time span with possible earthquake events coupled with rapid sedimentation (9 - 8.4 ka), and (f) the latest stage of the sedimentation and growth faulting with gradual sea level rise and stabilized (8.4 - 0 ka). Levels a to e are denoted in Fig. 5.

WK-1. It implies that during this 10000-year-long period the hanging wall had subsided enough to accumulate braid plain and flood plain fluvial growth sediments of while the Jingmei gravel would be exposed in the footwall and the extensional fault block region. In the meantime, sea level rose rapidly from -140 m (level a) to -55 m (level b) from ~18 to 12 ka (Fig. 5) during this period. So the elevation of the basin floor decreased drastically from 105 to 10 - 20 m high above the sea level from 23 to 12 ka.

(4) ~12 to 10 ka (Fig. 7d)

The situation over the next 2000 years in 12 - 10 ka was similar to the previous period as the sea level rose rapidly, except that the growth strata of fluvial deposits (middle part of Unit C3 of the Sungshan Formation) started to lap on to the area of the extensional fault block between the main and branch faults. This suggests that the subsidence in the extensional fault block region allowed fluvial sediments to accumulate. Sea level rose from -55 m (level b) to about -37 m (level c) during this period, while it still kept slightly lower than the basin ground.

(5) 10 to 8.4 ka (Fig. 7e)

The beginning of this period marked the onset of major marine incursions in the basin (Teng et al. 2000) as the sea level gradually rose from -37 m (level c) to -16 m (level e) from 10 to 8.4 ka. Sediments began to pile up across the entire section, and the accommodation space was filled contemporaneously with the rising sea level. Since then the regional topography should be very similar to the flat one

today, with less than 5 meters of difference in elevation between the borehole sites. The top horizons of C3 and C2 units, the estuarine deposits during that time, are therefore assumed to be similar in elevation along the Wuku profile in the three boreholes at around 9 and 8.4 ka, respectively. Accordingly, while the sea level continued to rise from level d to level e from 9 to 8.4 ka (Fig. 7e), we estimate that an extraordinarily rapid sedimentation of Unit C2 with 6.8, 10.1, and 17.4 m thickness at SCF-1, SCF-2, and WK-1, respectively. In the meantime, the Shanchiao Fault slipped vertically 3.3 m on the branch fault and 7.4 m on the main fault during the 600-year interval when C2 rapidly deposited in a relative deep, lower estuarine environment.

(6) 8.4 ka to present (Fig. 7f)

From 8.4 ka till present, as the sea level continued to rise from level e (-16 m) to present level and coupled with tectonic fault movement, the estuarine deposits of the C1 unit piled up and completed the uppermost sediments of the Taipei basin in the Wuku profile. The extensional fault block has been observed to subside (relative to the footwall) 7.8 meters and additional 11.3 meters for the hanging wall of the main fault.

6. DISCUSSION

6.1 Tectonic Loading Rates and Earthquake Events

Given that the rate of sediment supply and the rate of increasing accommodation space from rising sea level and tectonic subsidence are at balance, the sedimentation rate provides a direct way to estimate the effects of these components through time. When this is the case, sedimentation rate of growth strata across the fault offers explicit evaluation of both regional deposition rate and additional contribution from tectonic subsidence, with that obtained on the footwall containing only the former one.

Sedimentation rate investigation as described above is conducted on the C1 and C2 units of the Sungshan formation in the Wuku Profile, that is from 9 ka to present. The reason why constraining to the Holocene time is mainly because of the synchroneity of deposition and quality of age controls. We obtain the Holocene sedimentation rates (dividing the unit thickness by the time span of deposition) for three blocks: (a) derived from units on the footwall at SCF-1 block stand for the regional deposition rate, while (b) derived on the extensional fault block at SCF-2 and (c) the hanging wall block at WK-1 include excess rates representing tectonic subsidence. The estimations are presented in Table 4 and Fig. 8a.The yielded sedimentation rates are 1.7, 2.7, and 4.0 mm yr^{-1} for footwall, extensional fault block, and hanging wall, respectively, during 8.4 ka - present (C1 unit). However, we obtain a much higher sedimentation rate of 11.3, 16.8, and 29.2 mm yr^{-1} for footwall, extensional fault block, and hanging wall, respectively, during 9 - 8.4 ka (C2 unit). Note that difference in compaction rate of these Holocene units between the boreholes (i.e., different parts across the fault) would be well lower than 1 mm yr^{-1} (Meckel et al. 2006) and is thus ignored in the evaluation. By incorporating sea level rise, we obtain rate excess which we interpreted as tectonic subsidence rate (Table 4; Fig. 8a): 0.9 and 2.3 mm yr^{-1} for branch fault and main fault, respectively during 8.4 ka - present (C1 unit) and 5.5 and 17.8 mm yr^{-1} for branch fault and main fault, respectively during 9 - 8.4 ka (C2 unit).

Base on the above results, the period of 9 - 8.4 ka when C2 was laid is characterized by both rapid base level rise and high tectonic subsidence rate. Two paleo-earthquake events documented on the branch fault zone by Huang et al. (2007) coinciding the start and end of C2 deposition may lead to the much enhanced sedimentation rate and tectonic rate calculated. The total vertical tectonic subsidence of 3.3 and 7.4 m for branch and main fault during this period of 9 - 8.4 ka would mainly be subject to these two possible earthquake events. The rates derived from the C1 unit, embodying averages for a longer time period of 8.4 - 0 ka, are considered to better represent the Holocene and late Quaternary

Table 4. Sedimentation rate and inferred tectonic subsidence rate of the Shanchiao Fault zone in the Wuku Profile since ~9 ka (assuming negligible differences in compaction rates).

		Footwall (SCF-1)	Extensional fault block (SCF-1)	Hanging wall (WK-1)
C1 (~8.4 ka - present)	Thickness (m)	14.5	22.3	33.6
	Sedimentation rate (mm yr^{-1})	1.7	2.7	4
	Tectonic subsidence rate (mm yr^{-1})	-	0.9	2.3
C2 (~9 - ~8.4 ka)	Thickness (m)	6.8	10.1	17.5
	Sedimentation rate (mm yr^{-1})	11.3	16.8	29.2
	Tectonic subsidence rate (mm yr^{-1})	-	5.5	17.8

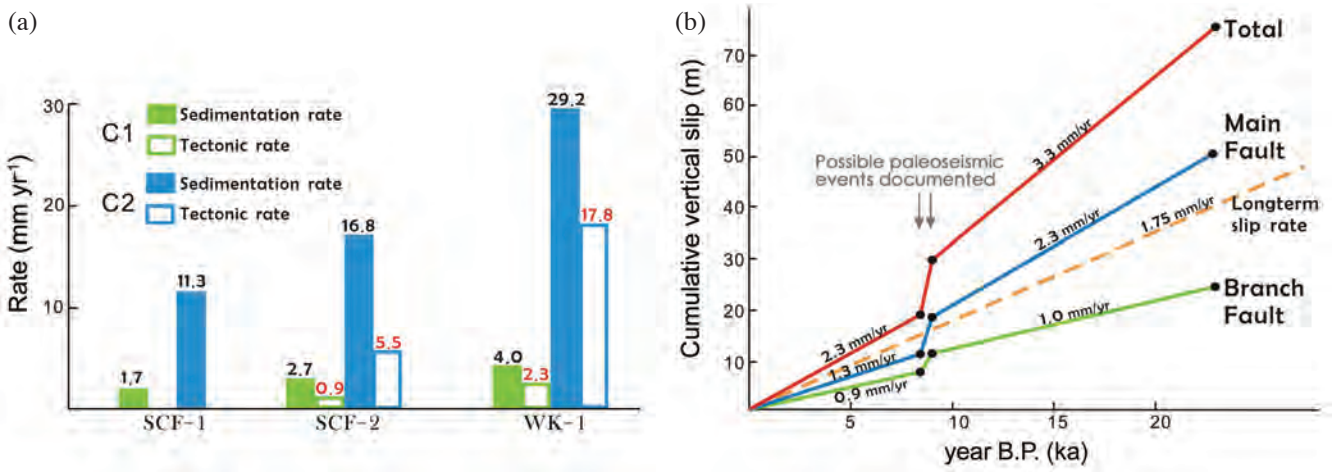

Fig. 8. (a) Sedimentation rate and tectonic subsidence rate of the C1 and C2 units at the Wuku boreholes. (b) Accumulative vertical slips for the Shanchiao fault since the LGM documented in the Wuku Profile.

long-term tectonic subsidence rate of the Shanchiao Fault which is 2.3 mm yr^{-1} on the hanging wall and 0.9 mm yr^{-1} on the extensional fault block, with a regional sedimentation rate of 1.73 mm yr^{-1}, and yield a rather high growth index (defined as fault throw rate divided by footwall sedimentation rate; Childs et al. 2003) of 1.3.

Tectonic subsidence rates of the Shanchiao Fault since 23 ka can also be inferred from vertical offsets of the horizons (Fig. 8b). Differences to the top depths of the Jingmei Formation (Unit C4) encompass the total vertical offsets of the Shanchiao Fault system since 23 ka, indicating the average vertical slip rates of 3.3 mm yr^{-1} with 1.1 mm yr^{-1} on the branch fault and 2.2 mm yr^{-1} on the main fault since the LGM. We also obtain about 1.0 and 2.3 mm yr^{-1} of averaged vertical slip rates on the branch and main faults, respectively, during 23 - 9 ka. The faulting rates obtained from various time periods and criteria are quite consistent with the exception of those from C2 unit. We can also conclude that the hanging wall down-throw rates were higher than the regional sedimentation rates since at least 9 ka.

Comparing to the long-term tectonic subsidence rate of the Shanchiao Fault, which was estimated to be 1.75 mm yr^{-1} since 0.4 Ma (Chen et al. 2007), the results of short-term rate of 3.3 mm yr^{-1} since 23 ka appears to be significantly higher (Fig. 8b). Although it is possible that the Shanchiao Fault has been more rigorous during the last tens of thousands of years, however, without study to complete the gap between 0.4 Ma and 23 ka, it is too early to draw a conclusion right now.

6.2 Correlation between Surface Topography and Subsurface Geology

Previous study of topographic mapping aiming at characterizing Shanchiao Fault zone geomorphology has identified a series of fault-related scarps arranged in an en-echelon array (Chen et al. 2006), which are present along the western edge of the Taipei Basin (Fig. 2a). The locations of fault-related scarps are generally in good agreement with existing borehole analyses which placed the surface trace of the Shanchiao Fault between borehole pairs including SCF-1 and 2, SCF-5 and 6, SCF-3 and 4 (Fig. 2a; Lin 2001; Huang et al. 2007). In the Wuku Profile, however, these traces and geomorphic features actually correspond to the branch fault zone; the main fault zone of the Shanchiao Fault may reach land surface east of SCF-2 where ground elevation is close to zero. We speculate that any topographic depressions caused by activities on the main fault zone would be readily erased since such troughs below the sea level tend to be rapidly filled by sediments given frequent typhoons and floods of Taiwan. This demonstrates that young faults without clear geomorphic evidence do not preclude the possibility of their recent activities, and hence the potential seismic threats.

Figure 9 shows a 3-D block diagram summarizing structural and geomorphic characteristics of the Shanchiao Fault zone. Structures of faulted and tilted strata within the basement rocks mainly reflect deformation features occurred in the mountain-building stage in the Taipei region consisting of thrust sheets, as the Hsinchuang Fault and the one seen in WK-1. The Hsinchuang Fault, by then the mountain frontal thrust some 2 Ma, only broke in the lower part of the Linkou Formation, and the basement rocks are buried within the fan-delta Linkou conglomerates (Teng et al. 2001). The uplift of the Linkou Tableland on the footwall block may be closely associated with the development of the normal faulting of the Shanchiao fault. The eastern border of the tableland, consisting of steep cliffs bearing some triangular facets and generally two threads of terraces (Chen et al. 2006), is composed of colluvial deposits with local outcrops of basement rocks (Teng et al. 2001). Geomorphic scarps bordering these terraces of uncertain origin might be related to past earthquake events as retreated fault scarps enhanced

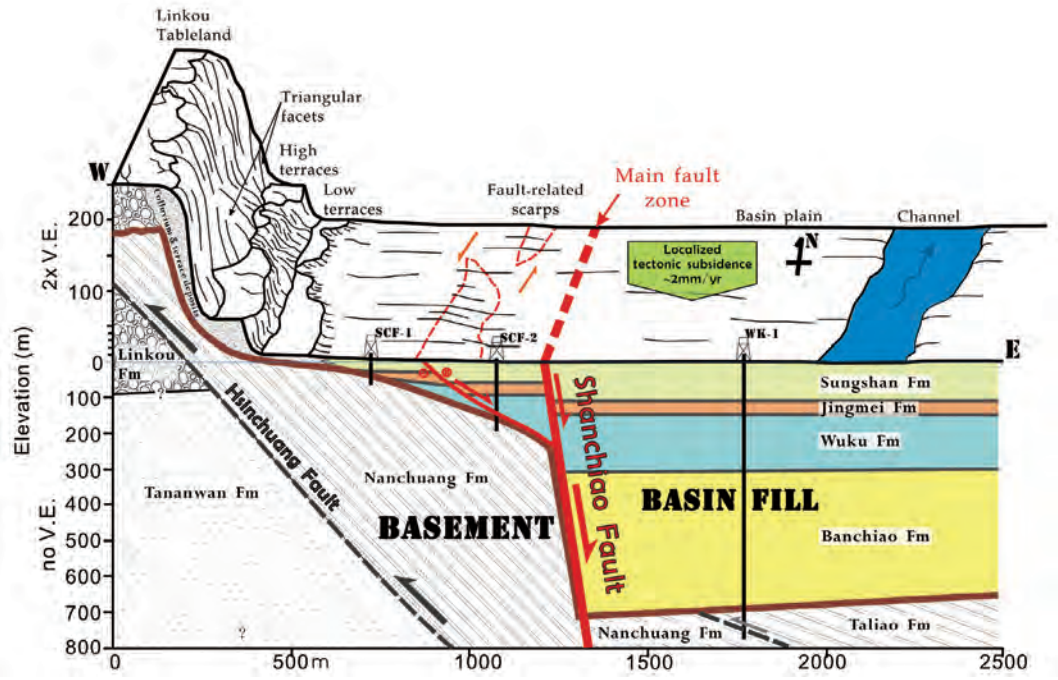

Fig. 9. Schematic 3-D diagram of the fault zone in the Wuku area, central portion of the Shanchiao Fault, displaying regional subsurface geology and its relation to surface topographic features.

by fluvial processes. The only in situ fault-related scarps are associated with the branch fault, and exhibit right-stepping segmentation which denotes sinistral transcurrent tectonic environment, in line with the fault striation recovered in the drilling hole (SCF-2; Lee et al. 1999) and with the regional GPS measurements (Rau et al. 2008).

7. CONCLUDING REMARKS

The Shanchiao Fault zone is interpreted to be composed of a main fault zone and a westerly shallower branch fault zone, with an extensional fault block in between. Left-lateral transcurrent motion in addition to normal faulting is present at least on the branch fault. The Shanchiao Fault has been highly active by almost incessant faulting since the Last Glacial Maximum of 23 ka. By comparing stratigraphy and its age, we are able to correlate stratigraphic units in a great detail across the three drilling holes along the Wuku profile. Under the assumption that the rapid rise of the sea level since the LGM would provide immense sediments to keep the topography flat in Taipei basin, we reconstructed the history of growth strata, which shows sedimentation significantly reflecting a combination effect of sea level rise and tectonic subsidence across the Shanchiao Fault since 23 ka. Furthermore, we calculated averaged vertical throw rates of about 2.2 and 1.1 mm yr^{-1} on the main and branch faults, respectively. The branch fault, corresponding to the major fault designated in previous documentations, made up about a third of total vertical displacement on the entire Shanchiao Fault zone since around 23 ka. Holocene tectonic subsidence rate of the fault appears to be similar and is constrained to be 2.3 mm yr^{-1} in the near-fault part of the hanging wall block, and 0.9 mm yr^{-1} in the extensional fault block area during 8.4 - 0 ka. However, an episode with possible two earthquake events revealed substantial tectonic subsidence of 7.4 and 3.3 m in the main fault and the branch fault, respectively, during a 600-yr time span of 9 - 8.4 ka. Presently, only the branch fault has geomorphic expressions; any topographic depressions caused by faulting on the main fault seem to be quickly filled. This has important implication for neotectonic investigations that faults of suspected status may still be active even though no clear direct geomorphic evidence can be found.

Acknowledgements This study was supported by the National Science Council of Taiwan (grant NSC 98-2116-M-001-011), Academia Sinica, and National Taiwan University. Special thanks to Louis S. Teng for very stimulating and knowledgeable discussions and comments. We are grateful to Yue-Gau Chen and Jyr-Ching Hu for their valuable comments and supports. Constructive reviews by Hao-Tsu Chu and Andrew T. Lin, which improved greatly the manuscript, are deeply appreciated. This is a contribution of the Institute of Earth Sciences, Academia Sinica, IESAS 1397.

REFERENCES

Angelier, J., E. Barrier, and H. T. Chu, 1986: Plate collision

and paleostress trajectories in a fold-thrust belt: The foothills of Taiwan. *Tectonophysics*, **125**, 161-178, doi: 10.1016/0040-1951(86)90012-0. [Link]

Brown, L. F., R. G. Loucks, R. H. Treviño, and U. Hammes, 2004: Understanding growth-faulted, intraslope subbasins by applying sequence-stratigraphic principles: Examples from the south Texas Oligocene Frio Formation. *AAPG Bull.*, **88**, 1501-1523, doi: 10.1306/07010404023. [Link]

Bull, J. M., P. M. Barnes, G. Lamarche, D. J. Sanderson, P. A. Cowie, S. K. Taylor, and J. K. Dix, 2006: High-resolution record of displacement accumulation on an active normal fault: Implications for models of slip accumulation during repeated earthquakes. *J. Struct. Geol.*, **28**, 1146-1166, doi: 10.1016/j.jsg.2006.03.006. [Link]

Caputo, R., B. Helly, S. Pavlides, and G. Papadopuolos, 2004: Palaeoseismological investigation of the Tyrnavos Fault (Thessaly, Central Greece). *Tectonophysics*, **394**, 1-20, doi: 10.1016/j.tecto.2004.07.047. [Link]

Chang, H. C., C. W. Lin, M. M. Chen, and S. T. Lu, 1998: An introduction to the active Faults of Taiwan, explanatory text of the active fault map of Taiwan. *Spec. Publ. Cent. Geol. Surv.*, **10**, 103 pp. (in Chinese)

Chen, C. T., K. H. Lin, Y. W. Jen, J. C. Lee, and Y. C. Chan, 2004 : Geomorphic studies of the Shanchiao Fault in the Taipei Basin, Xth Symposium on Quaternary of Taiwan, Taipei, Taiwan, 151-154.

Chen, C. T., J. C. Lee, J. C. Hu, Y. C. Chan, and C. Y. Lu, 2006: The active Shanchiao Fault in the Metropolitan Taipei area, Northern Taiwan: Geomorphic and geodetic analyses. *Eos, Trans., AGU*, **87-52**, Fall Meeting Supplement, Abstract T33D-0543.

Chen, C. T., J. C. Hu, C. Y. Lu, J. C. Lee, and Y. C. Chan, 2007: Thirty-year land elevation change from subsidence to uplift following the termination of groundwater pumping and its geological implications in the Metropolitan Taipei Basin, Northern Taiwan. *Eng. Geol.*, **95**, 30-47, doi: 10.1016/j.enggeo.2007.09.001. [Link]

Chen, W. F. and L. S. Teng, 1990: Depositional environment of Quaternary deposits of the Linkou Tableland, northwestern Taiwan. *Proc. Geol. Soc. China*, **33**, 39-63.

Chen, Y. G. and T. K. Liu, 1996: Sea level changes in the last several thousand years, Penghu Islands, Taiwan Strait. *Quat. Res.*, **45**, 254-262, doi: 10.1006/qres.1996.0026. [Link]

Childs, C., A. Nicol, J. J. Walsh, and J. Watterson, 2003: The growth and propagation of synsedimentary faults. *J. Struct. Geol.*, **25**, 633-648, doi: 10.1016/S0191-8141(02)00054-8. [Link]

Chiu, H. T., 1968: The Hsinchuang Fault in the Taoyuan area, northern Taiwan. *Proc. Geol. Soc. China*, **11**, 60-73.

Clark, J. A., W. E. Farrelle, and W. R. Peltier, 1978: Global changes in postglacial sea level: A numerical calculation. *Quat. Res.*, **9**, 265-287, doi: 10.1016/0033-5894(78)90033-9. [Link]

Dadson, S. J., N. Hovius, H. Chen, W. B. Dade, M. L. Hsieh, S. D. Willett, J. C. Hu, M. J. Horng, M. C. Chen, C. P. Stark, D. Lague, and J. C. Lin, 2003: Links between erosion, runoff variability and seismicity in the Taiwan orogen. *Nature*, **426**, 648-651, doi: 10.1038/nature02150. [Link]

Fairbanks, R. G., R. A. Mortlock, T. C. Chiu, L. Cao, A. Kaplan, T. P. Guilderson, T. W. Fairbanks, A. L. Bloom, P. M. Grootes, and M.-J. Nadeau, 2005: Radiocarbon calibration curve spanning 0 to 50000 years B.P. based on paired ^{230}Th/^{234}U/^{238}U and ^{14}C dates on pristine corals. *Quat. Sci. Rev.*, **24**, 1781-1796, doi: 10.1016/j.quascirev.2005.04.007. [Link]

Gawthorpe, R. and S. Hardy, 2002: Extensional fault-propagation folding and base-level change as controls on growth-strata geometries. *Sediment. Geol.*, **146**, 47-56, doi: 10.1016/S0037-0738(01)00165-8. [Link]

Ho, C. S., 1986: A synthesis of the geologic evolution of Taiwan. *Tectonophysics*, **125**, 1-16, doi: 10.1016/0040-1951(86)90004-1. [Link]

Hori, K., S. Tanabe, Y. Saito, S. Haruyama, V. Nguyen, and A. Kitamura, 2004: Delta initiation and Holocene sea-level change: Example from the Song Hong (Red River) delta, Vietnam. *Sediment. Geol.*, **164**, 237-249, doi: 10.1016/j.sedgeo.2003.10.008. [Link]

Hsieh, C. H., Y. F. Chang, and R. H. Sun, 1992: Seismic investigation of the Hsin-Chuan fault on the west of Taipei Basin. *Ti-Chih*, **12**, 13-26. (in Chinese)

Huang, S. Y., 2003: Prehistoric earthquakes along the Shanchiao Fault, Taipei Basin, Northern Taiwan. Master Thesis, Central Washington University, Washington, USA, 83 pp.

Huang, S. Y., C. M. Rubin, Y. G. Chen, and H. C. Liu, 2007: Prehistoric earthquakes along the Shanchiao fault, Taipei Basin, northern Taiwan. *J. Asian Earth Sci.*, **31**, 265-276, doi: 10.1016/j.jseaes.2006.07.025. [Link]

Hubert-Ferrari, A., J. Suppe, R. Gonzalez-Mieres, and X. Wang, 2007: Mechanisms of active folding of the landscape (southern Tian Shan, China). *J. Geophys. Res.*, **112**, B03S09, doi: 10.1029/2006JB004362. [Link]

Kao, H., S. S. J. Shen, and K. F. Ma, 1998: Transition from oblique subduction to collision: Earthquakes in the southernmost Ryukyu arc-Taiwan region. *J. Geophys. Res.*, **103**, 7211-7229, doi: 10.1029/97JB03510. [Link]

Lam, D. D. and W. E. Boyd, 2001: Some facts of sea-level fluctuation during the late Pleistocene-Holocene in Ha Long Bay and Ninh Binh area. *J. Sci. Earth*, **23**, 86-91.

Lee C. T. and Y. Wang, 1988: Quaternary stress changes in northern Taiwan and their tectonic implication, *Proc. Geol. Soc. China*, **31**, 154-168.

Lee, J. C., 1989: Neotectonics of northern Taiwan based on the faults and paleostress analyses. Master Thesis, National Taiwan University, Taipei, Taiwan, ROC, 128 pp. (in Chinese)

Lee, J. F., C. Z. Lin, D. C. Lai, T. W. Su, Z. L. Chiu, and C. J. Zeng, 1999 : The study on the formation of Taipei Basin. *Spec. Publ. Cent. Geol. Surv.*, **11**, 207-226. (in Chinese)

Lin, C. C., 1957: Geomorphology of Taiwan. Taiwan Province Literature Comunication, Taipei, 424 pp. (in Chinese)

Lin, C. W., H. C. Chang, S. T. Lu, T. S. Shih, and W. J. Huang, 2000: An Introduction to the Active Faults of Taiwan, 2nd Ed., Explanatory Text of the Active Fault Map of Taiwan. *Spec. Publ. Cent. Geol. Surv.*, **13**, 122 pp. (in Chinese)

Lin, C. Z., 2001: Geologic environment of the Taipei metropolis. Symposium on Geological Hazards in the Taipei Metropolis, 1-19. (in Chinese)

Lin, C. Z., 2005: Shanchiao Fault and the geological structures along the western margin of the Taipei Basin. Symposium on Volcanic Activities and the Shanchiao Fault in the Taipei Metropolis, 191-198. (in Chinese)

Lin, C. Z., T. C. Lai, L. Y. Fei, H. C. Liu, C. C. Chi, and T. W. Su, 1999: Results of deep borehole investigations in the Taipei Basin between 1992 to 1996. *Spec. Publ. Cent. Geol. Surv.*, **11**, 7-39. (in Chinese)

Lin, K. C., J. C. Hu, K. E. Ching, J. Angelier, R. J. Rau, S. B. Yu, C. H. Tsai, T. C. Shin, and M. H. Huang, 2010: GPS crustal deformation, strain rate, and seismic activity after the 1999 Chi-Chi earthquake in Taiwan. *J. Geophys. Res.*, doi: 10.1029/2009JB006417, in press.

Lu, C. Y., J. Angelier, H. T. Chu, and J. C. Lee, 1995: Contractional, transcurrent, rotational and extensional tectonics: Examples from Northern Taiwan. *Tectonophysics*, **246**, 129-146, doi: 10.1016/0040-1951(94)00252-5. [Link]

Machette, M. N., S. F. Personius, A. R. Nelson, D. P. Schwartz, and W. R. Lund, 1991: The Wasatch fault zone, Utah - Segmentation and history of Holocene earthquakes. In: Hancock, P. L., R. S. Yeats, and D. J. Sanderson (Eds.), Characteristics of Active Faults. *J. Struct. Geol.*, **13**, 137-149, doi: 10.1016/0191-8141(91)90062-N. [Link]

McCalpin, J. P. and S. P. Nishenko, 1996: Holocene paleoseismicity, temporal clustering, and probabilities of future large (M > 7) earthquakes on the Wasatch fault zone, Utah. *J. Geophys. Res.*, **101**, 6233-6253, doi: 10.1029/95JB02851. [Link]

Meckel, T. A., U. S. ten Brink, and S. J. Williams, 2006: Current subsidence rates due to compaction of Holocene sediments in southern Louisiana. *Geophys. Res. Lett.*, **33**, L11403, doi: 10.1029/2006GL026300. [Link]

Meghraoui, M., B. Delouis, M. Ferry, D. Giardini, P. Huggenberger, I. Spottke, and M. Granet, 2001: Active normal faulting in the upper Rhine Graben and paleoseismic identification of the 1356 Basel earthquake. *Science*, **293**, 2070-2073, doi: 10.1126/science.1010618. [Link]

Ota, Y. and J. Chappell, 1999: Holocene sea-level rise and coral reef growth on a tectonically rising coast, Huon Peninsula, Papua New Guinea. *Quat. Int.*, **55**, 51-59, doi: 10.1016/S1040-6182(98)00024-X. [Link]

Peng, C. H., L. S. Teng, and P. B. Yuan, 1999: Facies characteristics of Taipei Basin deposits. *Spec. Publ. Cent. Geol. Surv.*, **11**, 67-99.

Rau, R. J., K. E. Ching, J. C. Hu, and J. C. Lee, 2008: Crustal deformation and block kinematics in transition from collision to subduction: Global positioning system measurements in northern Taiwan, 1995-2005. *J. Geophys. Res.*, **113**, B09404, doi: 10.1029/2007JB005414. [Link]

Seno, T., 1977: The instantaneous rotation vector of the Philippine Sea Plate relative to the Eurasian Plate. *Tectonophysics*, **42**, 209-226, doi: 10.1016/0040-1951(77)90168-8. [Link]

Sharp, I. R., R. L. Gawthorpe, J. R. Underhill, and S. Gupta, 2000: Fault-propagation folding in extensional settings: Examples of structural style and synrift sedimentary response from the Suez rift, Sinai, Egypt. *Geol. Soc. Am. Bull.*, **112**, 1877-1899, doi: 10.1130/0016-7606(2000)112<1877:FPFIES>2.0.CO;2. [Link]

Shih, R. C., Y. H. Chan, and H. C. Liu, 2004: Shallow seismic reflection surveys of the Shanchiao Fault in the Guandu Plain. *Spec. Publ. Cent. Geol. Surv.*, **15**, 1-11. (in Chinese)

Shyu, J. B. H., K. Sieh, Y. G. Chen, and C. S. Liu, 2005: Neotectonic architecture of Taiwan and its implications for future large earthquakes. *J. Geophys. Res.*, **110**, B08402, 33 pp, doi: 10.1029/2004JB003251. [Link]

Song, S. R., S. J. Tsao, and H. L. Lo, 2000: Characteristics of the Tatun volcanic eruptions, north Taiwan: Implications for a cauldron formation and volcanic evolution. *J. Geol. Soc. China*, **43**, 361-378.

Suppe, J., 1981: Mechanics of mountain building and metamorphism in Taiwan. *Mem. Geol. Soc. China*, **4**, 67-89.

Taylor, S. K., A. Nicol, and J. J. Walsh, 2008: Displacement loss on growth faults due to sediment compaction. *J. Struct. Geol.*, **30**, 394-405, doi: 10.1016/j.jsg.2007.11.006. [Link]

Teng, L. S., 1990: Geotectonic evolution of late Cenozoic arc-continent collision in Taiwan. *Tectonophysics*, **183**, 57- 76, doi: 10.1016/0040-1951(90)90188-E. [Link]

Teng, L. S., 1996: Extensional collapse of the northern Taiwan mountain belt. *Geology*, **24**, 949-952, doi: 10.1130/0091-7613(1996)024<0949:ECOTNT>2.3.CO;2. [Link]

Teng, L. S., P. B. Yuan, and P. Y. Chen, 1993: Study on

stratigraphy and sedimentary environment. Report on Taipei Basin Subsurface Geology and Engineering Environment Research Project 1992, Central Geological Survey, MOEA, Taipei, Taiwan, ROC.

Teng, L. S., P. B. Yuan, P. Y. Chen, C. H. Peng, T. C. Lai, F. Y. Fei, and H. C. Liu, 1999 : Lithostratigraphy of the Taipei Basin deposits. *Spec. Publ. Cent. Geol. Surv.*, **11**, 41-66.

Teng, L. S., P. B. Yuan, N. T. Yu, and C. H. Peng, 2000: Sequence stratigraphy of the Taipei Basin deposits: A preliminary study. *J. Geol. Soc. China*, **43**, 497-520.

Teng, L. S., C. T. Lee, C. H. Peng, W. F. Chen, and C. J. Chu, 2001: Origin and geological evolution of the Taipei Basin, Northern Taiwan. *West. Pac. Earth Sci.*, **1**, 115-142.

Teng, L. S., T. K. Liu, Y. G. Chen, P. M. Liew, C. T. Lee, H. C. Liu, and C. H. Peng, 2004a: Influence of Tahan River capture over the Taipei Basin. *Geogr. Res.*, **41**, 61-78. (in Chinese)

Teng, L. S., C. T. Lee, P. M. Liew, S. R. Song, S. J. Tsao, H. C. Liu, and C. H. Peng, 2004b: On the Taipei dammed lake. *Geogr. Res.*, **36**, 77-100. (in Chinese)

van Wagoner, J. C., H. W. Posamentier, R. M. Mitchem, P. R. Vail, J. F. Sarg, T. S. Loutit, and J. Hardenbol, 1988: An overview of the fundamentals of sequence stratigraphy and key definitions. In: Wilgus, C. K., H. W. Posamentier, C. A. Ross, and C. G. St. C. Kendall (Eds.), Sea-Level Changes: An Integrated Approach, Society of Economic Paleontologists and Mineralogists Special Publication, **42**, 39-45.

Vergés, J., M. Marzo, and J. A. Muñoz, 2002: Growth strata in foreland settings. *Sediment. Geol.*, **146**, 1-9, doi: 10.1016/S0037-0738(01)00162-2. [Link]

Walia, V., T. C. Su, C. C. Fu, and T. F. Yang, 2005: Spatial variations of radon and helium concentrations in soil-gas across the Shan-Chiao fault, Northern Taiwan. *Radiat. Meas.*, **40**, 513-516, doi: 10.1016/j.radmeas.2005.04.011. [Link]

Wang, C. Y. and C. T. Sun, 1999: Interpretation of seismic stratigraphy in the Taipei Basin. *Spec. Publ. Cent. Geol. Surv.*, **11**, 273-292. (in Chinese)

Wang, W. S. and C. H. Chen, 1990: The volcanology and fission track age dating of pyroclastic deposits in Tatun volcano group, northern Taiwan. *Acta Geol. Taiwan.*, **28**, 1-40.

Wei, K., Y. G. Chen, and T. K. Liu, 1998: Sedimentary history of the Taipei Basin with constraints from thermoluminescence dates. *J. Geol. Soc. China*, **41**, 109-125.

Wernicke, B. and B. C. Burchfiel, 1982: Modes of extensional tectonics. *J. Struct. Geol.*, **4**, 105-115, doi: 10.1016/0191-8141(82)90021-9. [Link]

Woodcock, N. H. and C. Schubert, 1994: Continental strike-slip tectonics. In: Hancock, P. L. (Ed.), Continental Deformation, Pergamon Press, New York, 251-263.

Woodroffe, S. A. and B. P. Horton, 2005: Holocene sea-level change in the Indo-Pacific. *J. Asian Earth Sci.*, **25**, 29-43, doi: 10.1016/j.jseaes.2004.01.009. [Link]

Wu, F. T., 1965: Subsurface geology of the Hsinchuang structure in the Taipei Basin. *Petrol. Geol. Taiwan*, **4**, 271-282.

Wu, F. T., R. J. Rau, and D. Salzberg, 1997: Taiwan orogeny: Thin-skinned or lithospheric collision? *Tectonophysics*, **274**, 191-220, doi: 10.1016/S0040-1951(96)00304-6. [Link]

Yeh, Y. H., E. Barrier, C. H. Lin, and J. Angelier, 1991: Stress tensor analysis in the Taiwan area from focal mechanisms of earthquakes. *Tectonophysics*, **200**, 267-280, doi: 10.1016/0040-1951(91)90019-O. [Link]

Yokoyama, Y., Y. Kido, R. Tada, I. Minami, R. C. Finkel, and H. Matsuzaki, 2007: Japan Sea oxygen isotope stratigraphy and global sea-level changes for the last 50000 years recorded in sediment cores from the Oki Ridge. *Palaeogeogr. Palaeoclimatol. Palaeoecol.*, **247**, 5-17, doi: 10.1016/j.palaeo.2006.11.018. [Link]

Yu, S. B., H. Y. Chen, and L. C. Kuo, 1997: Velocity field of GPS stations in the Taiwan area. *Tectonophysics*, **274**, 41-59, doi: 10.1016/S0040-1951(96)00297-1. [Link]

Yu, S. B., H. Y. Chen, L. C. Kou, C. S. Hou, and C. F. Lee, 1999: A study on the fault activities of the Taipei Basin. *Spec. Publ. Cent. Geol. Surv.*, **11**, 227-251.